https://doi.org/10.1016/j.jcat.2016.09.017


# A cascading gradient pore microstructured photoanode with enhanced photoelectrochemical and photocatalytic activities

Lin Li[a,b], Rong Chen[a,b]*, Xun Zhu[a,b]**, Qiang Liao[a,b], Hong Wang[a,b], Liang An[c], Muxing Zhang[a]

[a] Key Laboratory of Low-grade Energy Utilization Technologies and Systems (Chongqing University), Ministry of Education, Chongqing 400030, China

[b] Institute of Engineering Thermophysics, Chongqing University, Chongqing 400044, China

[c] Department of Mechanical Engineering, The Hong Kong Polytechnic University, Hung Hom, Kowloon, Hong Kong, China

*Corresponding author. Tel.: 0086-23-65103119; fax: 0086-23-65102474; e-mail: rchen@cqu.edu.cn

**Co-corresponding author. Tel.: 0086-23-65102474; fax: 0086-23-65102474; e-mail: zhuxun@cqu.edu.cn

## Abstract

In this work, a novel photoanode with a cascading gradient pore microstructure is proposed to enhance photoelectrochemical and photocatalytic activities, which consists of a nanocrystalline $TiO_2$ layer synthesized by the sol-gel method, a microporous layer and a macroporous layer formed by adding PEG and PMMA as the template, respectively. The gradient pore microstructure can not only enhance the mass and photon transfer and improve the light utilization, but also increase the electrical conductivity and restrain the recombination of photo-excited electron-hole pairs. Furthermore, the cascading design helps to establish tighter interparticle connections between each layer. Because of these merits, it has been found that the cascading gradient pore microstructured photoanode exhibited a 63% improvement

compared to the conventional photoanode in terms of photoelectrochemical activity. Besides, this new design also enhanced the photocatalytic activity, leading to a much higher methylene blue degradation efficiency of 76.7% than that of conventional photoanode (62.5%). The effect of the PMMA/$TiO_2$ ratio on the structural and performance characteristics of the proposed photoanode was also investigated. The highest performance was achieved with the PMMA/$TiO_2$ ratio of 1:1. The obtained results create a new avenue for designing the photoanode of the photoelectrochemical systems.

***Keywords*:** Photoanode; cascading gradient pore microstructure; photocatalytic fuel cell; photoelectrochemical and photocatalytic activities; PMMA/$TiO_2$ ratio

## 1. Introduction

As one of typical photoelectrochemical systems, photocatalytic fuel cells (PFCs) that integrate the photocatalytic oxidation and fuel cell technologies have become an advanced research area in recent years [1-4]. Upon illumination, the photosensitive semiconductors at the photoanode of PFCs generate the electron-hole pairs with greater photonic energy than its band gap. Photo-initiated holes that have strong oxidation ability are then to degrade most organics while electrons flow to the counter electrode to generate electricity. By this way, the chemical energy contained in energy-rich wastewater can be recovered to available energy along with organic contaminant degradation. Therefore, PFCs can help to alleviate both energy shortage and environmental contamination issues facing our planet by degrading pollutants and simultaneously generating electricity [5]. Moreover, PFCs feature wild operation conditions, low secondary pollution and easily-controlled reaction, making it a promising application prospect [6-9].

At present, $TiO_2$ has been the most widely used as photocatalysts of PFCs due to its high activity, non-toxicity, low cost, and chemical inertness [10]. To prepare the photoanodes, $TiO_2$ is usually in the form of a thin film by applying $TiO_2$ to conductive glass via various methods [11-13], such as the screen-printing method, doctor-blade technique, wet spraying method, etc. However, the $TiO_2$ films formed by these methods usually exhibit small specific surface area and poor photon and mass transfer, which highly constrain its photoelectrochemical and photocatalytic activities.

Hence, in order to alleviate this problem, much attempt has been undertaken to ameliorate the spatial structure of the photoanode [14-15]. One common method is the in-situ growth of $TiO_2$ nanorods, nanotubes, nanowires, etc. [16-18], which have been found to be able to dramatically improve the specific surface area and mass transfer. For instance, Liu et al. [19] prepared a short $TiO_2$-nanotube-array and applied it to PFCs. Compared with conventional $TiO_2$ films that were stacked by $TiO_2$ nanoparticles, the nanotube-array structure demonstrated improved photoelectrochemical performance. However, the in-situ growth of $TiO_2$ is usually conducted on a Ti based substrate. Such manner is difficult to be realized on the conductive glass and also complicated for manufacturing. Another approach to ameliorate the spatial structure of the photoanode is to construct porous $TiO_2$ films using polystyrene (PS), poly(methyl methylacrylate) (PMMA), octadecylamine (ODA) or other microspheres as templates [20]. In 2010, Kamegawa et al. [21] successfully prepared a $TiO_2$ film with uniform pores by using PMMA as the template. As compared to traditional dense $TiO_2$ film, it was found that this porous structure provided superior photocatalytic degradation efficiency to 2-propanol and acetaldehyde. Zhang et al. [22] utilized ODA as the template to synthesize porous $TiO_2$ film by a sol-gel method and confirmed that this porous structure was superior in methyl orange degradation. However, although these porous $TiO_2$ films have shown good performance in the photocatalytic wastewater treatment, when these porous $TiO_2$ films were applied to the glossy surface of the conductive glass that was commonly used as the photoanode substrate of PFCs, they might be easily peeled off

due to the voids and shrunk contact area with the substrate [23]. In short, it is essential to develop a high-efficiency photoanode for improving the PFC performance.

It has been known that the complicated multiple processes are involved in the photoanode, including the photon receipt, electron-hole pair generation and mass and photon transport. A high-efficiency photoanode should have the following features: large specific surface area, high mass transfer efficiency, effective electron transfer pathways along with improved photon transfer ability for light harvesting. The above literature review indicates that the existing photoanodes are hardly to fulfill these requirements. Therefore, a novel photoanode with a cascading gradient pore microstructure was proposed in this work. As illustrated in Fig. 1, the cascading gradient pore microstructured photoanode consists of three layers on the FTO conductive glass: a nanocrystalline $TiO_2$ layer at the bottom, a microporous $TiO_2$ layer in the middle and a macroporous $TiO_2$ layer at the top. Such a cascading gradient pore microstructure offers the desired features for the photoanode. First, the top macroporous $TiO_2$ layer provides sufficient light-transfer path and facilitates the light scattering, thus allowing incident photon flux to be efficiently absorbed. In addition, it can also provide large specific surface area for the photoelectrochemical reaction and small transport resistance for facilitating the mass transfer of organic fuels and ions. For the middle microporous $TiO_2$ layer, it can not only provide efficient diffusion pathways for mass transfer but also help to trap the incident photons. The bottom nanocrystalline layer ensures strong adhesion to the electrode substrate, provides high conductivity and prevents the recombination of photo-excited

electron-hole pairs. Furthermore, the cascading design can avoid the direct contact between two layers with large pore size difference, helping to establish tighter interparticle connections between these layers and enhancing the electron transport from the external porous network structure to the internal electrode substrate. As a result, all these features of this novel photoanode will favor its performance.

In line with this idea, we developed this novel photoanode layer by layer. From the bottom to up, these three layers with different pore structures were fabricated subsequently onto the FTO conductive glass. (i) A nanocrystalline $TiO_2$ layer was firstly deposited on the FTO conductive glass by the sol-gel method, termed as NC. (ii) A microporous $TiO_2$ layer was then fabricated on the top of the nanocrystalline $TiO_2$ layer by the wet spray method using polyethylene glycol (PEG) as template to form micropores, termed as $TiO_2$. (iii) Finally, a macroporous $TiO_2$ layer was formed on the top by spraying the $TiO_2$ colloid with the addition of a poly (methyl methylacrylate) (PMMA) template (1.8 μm in diameter) to form macropores, termed as PMMA. As such, a novel photoanode with a cascading gradient pore microstructure, termed as NC/$TiO_2$/PMMA, could be developed. Both the photoelectrochemical and photocatalytic activities of the fabricated novel photoanode were evaluated. The role of each layer in this design was also elaborated. In particular, the effect of the $TiO_2$/PMMA ratio on the structural and performance characteristics of the developed photoanode was also investigated. Results showed that this novel photoanode could greatly enhance the photoelectrochemical and photocatalytic activities, which provides a potential direction for the future development of the

photoanode.

## 2. Materials and methods

### 2.1 Preparation of the cascading gradient pore microstructured photoanode

The cascading gradient pore microstructured photoanode, which consisted of a nanocrystalline $TiO_2$ layer at the bottom, a microporous $TiO_2$ layer in the middle and a macroporous layer $TiO_2$ at the top, was prepared on a FTO conductive glass. The bottom densely packed nanocrystalline $TiO_2$ layer was firstly synthesized by the sol-gel method onto the FTO conductive glass cleaned by sonication in acetone, isopropanol and ethanol. The procedure was presented as follows [24]. 3.5 g of the nonionic surfactant Triton X-100 (Sigma-Aldrich, USA) was firstly mixed with 19 mL of ethanol. Then, 3.4 mL of glacial acetic acid (Aladdin, China) and 1.8 mL of titanium tetraisopropoxide (Aladdin, China) were added with vigorous stirring. After stirring, the prepared colloid was applied on the FTO conductive glass by the dipping method and dried in air for a few minutes and finally calcined at 550$^{o}$C for 10 minutes with the temperature ramp of 20$^{o}$C min$^{-1}$ to form a nanocrystalline $TiO_2$ layer. On the top of the nanocrystalline $TiO_2$ layer, the microporous layer was formed by the wet spraying method with the $TiO_2$ colloid. The $TiO_2$ colloid was prepared by the common sol-gel method [25]. 6 g $TiO_2$ nanoparticles (Aeroxide P25, Acros, Belgium) were dispersed in a mixture of 60 ml DI. 0.1 mL of a Triton X-100 (Sigma-Aldrich, USA) and 1.2 g polyethylene glycol (PEG2000, Aladdin, China) was added and mixed for 12 hours. The prepared $TiO_2$ colloid was then diluted with ethanol and applied on the top of the nanocrystalline $TiO_2$ layer by an air spray gun. The $TiO_2$

loading of the microporous layer was kept at 0.2 mg $cm^{-2}$. The top macroporous $TiO_2$ layer was prepared using $TiO_2$ colloid and PMMA microspheres with 1.8 μm in diameter (Soken Chemical and Engineering Co., Japan) as a template. The PMMA microspheres were added into the $TiO_2$ colloid. 2.5 g of PMMA microspheres were dispersed in 20 ml of distilled water containing 6 wt% of polyvinyl alcohol (PVA, Aladdin, China) and then stirred at 95°C in the oil bath for 2 hours. After that, the prepared PMMA aqueous solution was introduced into the $TiO_2$ colloid at various proportions. After 24 h stirring at room temperature, the resulting suspension was deposited onto the substrate by the wet spraying. After drying at 80°C in air, all samples were calcined at 550°C for 2 h to remove the PMMA templates. In addition, for verifying the role of each layer, we also fabricated the single-layer photoanode with a microporous layer (termed as $TiO_2$), the bilayer photoanode with the nanocrystalline $TiO_2$ layer and the microporous layer (termed as NC/$TiO_2$) and the bilayer photoanode with the nanocrystalline $TiO_2$ layer and the macroporous layer (termed as NC/PMMA). For fair comparison, the total photocatalyst loadings of all prepared photoanodes were kept at 1 mg $cm^{-2}$.

**2.2 Photoelectrochemical measurements**

The photoelectrochemical characterizations were carried out in a quartz electrochemical pool with three-electrode configuration at room temperature. A 300 W xenon lamp (CEL-HXF300, Aulight, China) with an AM 1.5G filter was used as a light irradiation source to provide the irradiance intensity of 100 mW $cm^{-2}$. The three-electrode system consisted of a Pt counter electrode, an Ag/AgCl reference

electrode and the prepared photoanode as the working electrode. The effective surface area of the working electrode was 1.0 × 1.0 = 1.0 $cm^2$. The fuel contained 0.2 M KOH as the electrolyte and 10% ethanol in volume. Photocurrent, linear sweep voltammetry (LSV) and electrochemical impedance spectroscopy (EIS) were measured by an electrochemical station (Parstat MC, Princeton Applied Research, USA). The chronoamperometry curves of the photoanodes were obtained at 0 V versus Ag/AgCl. The linear sweep voltammograms were operated at 10 mV $s^{-1}$ in a potential range of −1.0 to +0.6 V versus Ag/AgCl. EIS measurements were performed with an AC amplitude of 10 mV and the frequency ranging from 100 kHz to 0.1 Hz.

**2.3 Photocatalytic measurement**

In addition to the photoelectrochemical measurements, the photocatalytic activities of the prepared photoanodes were also evaluated via the degradation of methylene blue (MB) with an initial concentration of $3\times10^{-5}$ M. MB is a common residual in wastewater from the textile industry, thus being used as a model contaminant in this work. Prior to the testing, MB was firstly dissolved into distilled water and the pH value was maintained at 7.0. All the sampling photoanodes with the identical area of 10 $cm^2$ were then placed in a 25-mL quartz beaker with magnetic stirring to degrade MB. The MB concentrations were determined by the absorption spectra using an UV−visible spectrophotometer (TU-1901, Persee, China) at a wavelength of 664 nm, which corresponded to the absorbance peak of MB. The MB concentrations during the experiments were monitored at every interval of 10 min.

## 3. Results and discussion

### 3.1 Morphology characterization

The morphologies of the sampling photoanodes were characterized by scanning electron microscopy (S4800-SEM, Hitachi, Japan). Fig. 2a shows a cross-section image illustrating the cascading gradient pore microstructured photoanode with the $TiO_2$/PMMA ratio of 1:1 at the macroporous layer. From the bottom to up, the nanocrystalline $TiO_2$ layer, the microporous $TiO_2$ layer and the macroporous $TiO_2$ layer exhibited visible difference in the pore structure. Clear boundaries can be identified at the interfaces between these layers. The thicknesses of the macroporous $TiO_2$ layer and microporous $TiO_2$ layer were approximately 12 μm and 3 μm, respectively. Obviously, the microporous layer is much thinner than the macroporous layer. Such design is able to reduce the light attenuation in the catalyst layer. This is because the propagation of the irradiated light toward and within the photoanode can then be described by the Beer–Lambert law for homogeneous semiconductor films [26]. The change in the light intensity shows an exponential decrease with the penetration depth, and the extinction coefficient of the material defines the extent of this decay. In this case, the light attenuation in the microporous layer is very serious so that this layer should be designed to be thinner to some extent. For the top layer shown in Fig. 2a, it can be seen that the top layer comprised a porous coral structure. The formed macropores were randomly dispersed in this layer with the diameter approximately corresponding to the PMMA microsphere diameter of 1.8 μm. Besides,

some disordered large pores with the pore size larger than the PMMA microsphere size were also observed. This is because when the PMMA template was removed during the thermal treatment at 550$^{o}$C, the solidification and collapsion of the $TiO_2$ solid framework increased the pore size. All these macropores could provide both the ideal photon harvester and light path for initiating photocatalytic reactions because it could not only offer more paths for photons but also act as the center for light scattering. Moreover, the existence of macropores can increase the reaction area and promote the mass transfer to allow more reactants to be involved. Different from the macroporous layer, densely-packed $TiO_2$ P25 nanoparticles with numerous micropores were clear to be seen in the middle porous layer. These micropores could not only provide sufficient pathways for mass and electrons and trap the incident photons efficiently but also help to establish tighter interparticle connections between the top macroporous layer and bottom nanocrystalline layer. As for the bottom nanocrystalline layer, because it was rather thin, a high-resolution SEM was performed to characterize the bottom nanocrystalline layer. The result is presented in Fig. 2b, which shows a cross-sectional image of the synthesized nanocrystalline $TiO_2$ layer on the FTO conductive glass. It can be seen that the nanocrystalline $TiO_2$ layer with the approximate thickness of about 170 nm was densely deposited on the FTO layer with the thickness of approximately 700 nm. Such a dense structure ensures this photoanode to be strongly adhered to the electrode substrate. Fig. 3 shows the top-view surface morphologies of the nanocrystalline $TiO_2$ layer, microporous $TiO_2$ layer and macroporous $TiO_2$ layer, respectively. It can be seen that the surface of the

nanocrystalline $TiO_2$ layer was rather smooth and dense (Fig. 3a), while the surface of the microporous layer was relatively rough and distributed with some disordered micropores (Fig. 3b). For the top layer, many macropores were distributed throughout the surface of the photoanode (Fig. 3c). The pore size well responded to the diameter of the PMMA microspheres but the surface was much rougher than the other two layers. In addition, because of the thermal treatment at high temperature, some distortion and defects were also observed. In summary, the above SEM results fully demonstrate the formation of the novel photoanode with the cascading gradient pore microstructure.

**3.2 Photoelectrochemical activity characterization**

With the prepared NC/$TiO_2$/PMMA photoanode, the photoelectrochemical activity was characterized. In addition, to provide a deep insight into the function of each layer in the proposed photoanode, the conventional single-layer $TiO_2$ photoanode and two bilayer $TiO_2$ photoanodes of the NC/$TiO_2$ and NC/PMMA were also tested and compared. Fig. 4a shows the light responses of the $TiO_2$, NC/$TiO_2$, NC/PMMA and NC/$TiO_2$/PMMA photoanodes. As shown, all photoanodes could immediately respond to the light illumination. In a few seconds, the photocurrents reached the steady values. The photocurrents could be reproducible when the light was periodically switched from the light off to the light on with a 60/60 s light/dark interval, forming a rectangle pulse signal. Although all photoanodes could well respond to the light illumination, the photocurrent density of the conventional $TiO_2$ photoanode was only 0.27 mA $cm^{-2}$, which was much lower than those of the other

three photoanodes. This result indicates that the addition of a nanocrystalline $TiO_2$ layer led to a notable increase in the current density because of strong adhesion, which enhanced the electron transport and prevented the recombination of the electron-hole pairs. More promisingly, the photocurrent of the NC/$TiO_2$/PMMA photoanode was 0.44 mA $cm^{-2}$, which was much higher than those of the NC/$TiO_2$ and NC/PMMA photoanodes. The 22% and 47% improvements in the photocurrent as compared to the NC/$TiO_2$ and NC/PMMA photoanodes were achieved, respectively. Many aspects contributed to the greatly-enhanced photoelectrochemical activity of this novel photoanode. First, the macroporous layer could facilitate the mass transport and provide large specific surface area for the photoelectrochemical reactions. Second, macropores could not only offer more paths for photons but also serve as light scattering center to deliver photons to the photocatalysts in the photoanode. Third, the microporous layer could provide large specific surface area for the photoelectrochemical reactions and transport paths for the mass and photon. Forth, the microporous layer located in the middle could establish tighter interparticle connections between the top and bottom layers, helping to overcome the drop-off of the macroporous $TiO_2$ layer and enhancing the electron transport from the external porous network to the internal. Because of the above reasons, the proposed gradient pore microstructured photoanode exhibited the best performance among these photoanodes.

To further elaborate the roles of the microporous layer and macroporous layer. Attention is now paid to the comparison of the NC/$TiO_2$ and NC/PMMA photoanodes.

It can be found that the NC/PMMA photoanode only yielded 0.3 mA $cm^{-2}$, which was much lower than that of the NC/$TiO_2$ photoanode. It is implied that although the NC/PMMA photoanode could greatly improve the mass transport and provide more paths for photons, the absence of the middle microporous layer, *i.e.*, the sole existence of macropores led to inefficient light harvesting because the photons might be directly scattered. As a result, the photoelectrochemical activity was lowered. Moreover, the direct contact between the nanocrystalline $TiO_2$ layer and macroporous $TiO_2$ layer was not beneficial for the electron migration between these two layers and made the macroporous $TiO_2$ layer to be easily dropped off from the nanocrystalline $TiO_2$ layer, which also decreased the performance. Therefore, the microporous layer plays a significant role in trapping the photons for the photoelectrochemical reactions and electron migration.

Figure 4b shows the I−V characteristics of the $TiO_2$, NC/$TiO_2$, NC/PMMA and NC/$TiO_2$/PMMA photoanodes. It is seen that the conventional $TiO_2$ photoanode exhibited a very low photocurrent, whereas the photocurrents of other samples were obviously enhanced in the entire scanning region, which highlighted the advantages of the nanocrystalline $TiO_2$ layer. Similar to the light responses of these photoanodes, the performance sequentially decreased from the NC/$TiO_2$/PMMA, NC/$TiO_2$, NC/PMMA to the $TiO_2$ photoanodes. As an example, at an applied potential of −0.3 V versus Ag/AgCl, their corresponding current densities were 0.47 mA $cm^{-2}$, 0.38 mA $cm^{-2}$, 0.33 mA $cm^{-2}$ and 0.29 mA $cm^{-2}$, respectively. The cascading gradient pore microstructured photoanode showed the highest current density. Moreover, the onset

potentials of these photoanodes were also different. For the $TiO_2$, NC/$TiO_2$ and NC/PMMA photoanodes, the onset potentials of them were around −0.95 V, −0.97 V and −0.93 V, respectively, while the onset potential of the NC/$TiO_2$/PMMA photoanode was −0.99 V. The proposed photoanode showed more negative onset potential. The increased current density and lowered onset potential further represent the promotion in the photoelectrochemical activity of the cascading gradient pore microstructured photoanode.

To further understand the mechanism leading to the improvement in the photoelectrochemical activity of this novel photoanode, the EIS measurements were also carried out to evaluate the charge transfer resistance of these photoanodes. Fig. 4c shows the EIS (Nyquist plots) results of these photoanodes at the open circuit voltage under illumination. As known, the charge transfer resistance ($R_{ct}$), which can reflect the electron and hole transport as well as the ion transport in the photoanode, can be calculated by fitting the semi-arc at low frequency region [27]. Small circular radius represents low electron transfer resistance and high separation efficiency of the photogenerated electrons and holes [28]. Thus, $R_{ct}$ can be used to judge how the change transfer affects the rate of the photoelectrochemical reaction. As seen from Fig. 4c, the charge transfer resistances of the NC/$TiO_2$, NC/PMMA and NC/$TiO_2$/PMMA photoanodes were smaller than that of the single-layer $TiO_2$ photoanode without the nanocrystalline $TiO_2$ layer, demonstrating that the nanocrystalline $TiO_2$ layer can effectively facilitate the electron transfer and restrain the recombination of photogenerated electron-hole pairs. More obviously, the $R_{ct}$ of the NC/$TiO_2$/PMMA

photoanode was much lower than those of the NC/$TiO_2$ and NC/PMMA. The outstanding reduction in $R_{ct}$ for the NC/$TiO_2$/PMMA photoanode indicates that the considerably fast photoelectrochemical reaction rate and the reduced interfacial charge transfer resistance were achieved. However, the $R_{ct}$ of the NC/PMMA photoanode was higher than that of the NC/$TiO_2$ photoanode, implying that the electron transfer resistance was large. This is mainly attributed to the decreased contact area of between the macroporous layer and the bottom layer, further demonstrating that directly coating the macroporous layer onto the nanocrystalline layer was not preferable for effective electron transfer. Besides, such design may cause the macroporous layer to be easily peeled off. As a result, the NC/PMMA photoanode exhibited lower photocurrent than did the NC/$TiO_2$ photoanode. However, for the cascading gradient pore microstructured photoanode, the gradual decrease of the pore size could dramatically solve this problem. Therefore, the NC/$TiO_2$/PMMA photoanode showed the lowest impedance and the best performance.

### 3.3 Photocatalytic activity characterization

In addition to the photoelectrochemical activity characterization, the photocatalytic activity of the cascading gradient pore microstructured photoanode was also assessed in terms of the degradation efficiency of MB. As shown in Fig. 5a, for all photoanodes, the MB concentrations were decreased upon prolonged irradiation time. The MB degradation profiles obtained with different designs ($TiO_2$, NC/$TiO_2$, NC/PMMA, NC/$TiO_2$/PMMA) were compared, among which the NC/$TiO_2$/PMMA photoanode exhibited the highest photocatalytic activity. Under the irradiation for 40 min, the MB

degradation efficiency of 62.5%, 64.6% and 70.0% were obtained for the $TiO_2$, NC/$TiO_2$ and NC/PMMA photoanodes, respectively, while the developed NC/$TiO_2$/PMMA photoanode yielded the highest MB degradation efficiency of 76.7%. Meanwhile, the photodegradation of MB can be assumed to follow a pseudo-first-order reaction, and its kinetics can be expressed as follows [29]:

$$-ln(C_t/C_0) = kt \quad (1),$$

where $k$ is the apparent reaction rate constant ($min^{-1}$), $t$ is the irradiation time and $C_0$ and $C_t$ stands for the initial MB concentration and the concentration corresponding to the irradiation time of $t$, respectively. From the plots of $-ln(C_t/C_0)$ versus the irradiation time (Fig. 5b), the degradation rate constants fitted from the slopes of these straight lines were $3.61\times10^{-2}$, $3.00\times10^{-2}$, $2.60\times10^{-2}$ and $2.48\times10^{-2}$ $min^{-1}$ for the NC/$TiO_2$/PMMA, NC/PMMA, NC/$TiO_2$ and $TiO_2$ photoanodes, respectively. It can be found that not only the MB degradation efficiency but also the photodegradation rate constant of the NC/$TiO_2$/PMMA photoanode were much higher than the other samples, indicating the superior photocatalytic activity of the cascading gradient pore microstructured photoanode. This can be partially attributed to (i) the enhanced photon transfer derived from the formed macropores and micropores, which can trap more photons to increase the light utilization; (ii) enhanced mass transport due to the macropores; and (iii) large specific surface area for the photocatalytic reactions. Interestingly, it can also be found that although the NC/$TiO_2$ photoanode yielded better photoelectrochemical activity than did the NC/PMMA photoanode, the photodegradation rate constant of the NC/PMMA was much higher than that of the

NC/$TiO_2$ photoanode in the photocatalytic activity measurements. In addition, the NC/$TiO_2$ and $TiO_2$ photoanodes showed a slight difference in the MB degradation efficiency and photodegradation rate constant. This implies that the bottom nanocrystalline $TiO_2$ layer has little contribution on the photocatalytic activity and mainly contributes to the electron transfer.

### 3.4 Effect of the PMMA/$TiO_2$ ratio

Since the microstructure of the macroporous layer highly depends on the content of the added PMMA, the effect of the PMMA/$TiO_2$ ratio on the performance of the cascading gradient pore microstructured photoanode was investigated. Four photoanodes with the PMMA/$TiO_2$ ratio ranging from 1:5, 1:2, 1:1 to 2:1 were prepared with an identical $TiO_2$ loading of 1 mg $cm^{-2}$. Fig. 6 shows the SEM top view and cross-sectional view of these samples with the PMMA/$TiO_2$ ratios of 1:5, 1:2 and 2:1, which displayed distinct differences in both pore quantity and distribution. As shown, at the lowest PMMA/$TiO_2$ ratio of 1:5, only a few macropores were presented on the surface of the photoanode and these macropores were distributed randomly (see Fig. 6a). High PMMA/$TiO_2$ ratio of 1:2 could create more macropores (see Fig. 6b). At the highest PMMA/$TiO_2$ ratio of 2:1, a large amount of macropores were distributed uniformly (see Fig. 6c). These SEM images revealed that the number of macropores increased as the PMMA/$TiO_2$ ratio increased from 1:5 to 2:1 because more PMMA microspheres were removed during the thermal treatment. As a result, higher ratio generated more voids and thinner solid framework. Notably, the macropores were poorly formed at extremely high PMMA/$TiO_2$ ratio because

insufficient solid content was remained when the template was removed after calcining, making the macroporous layer to be easily cracked and even peeled off.

The light responses of the cascading gradient pore microstructured photoanodes with different PMMA/$TiO_2$ ratios were accessed and the results are shown in Fig. 7a. The photocurrents significantly increased from 0.37 mA $cm^{-2}$ to 0.44 mA $cm^{-2}$ upon illumination when the PMMA/$TiO_2$ ratio was increased from 1:5 to 1:1. However, when the PMMA/$TiO_2$ ratio was further increased to 2:1, the photocurrent was markedly reduced, which was even lower than those of the NC/$TiO_2$ photoanode and the photoanode with the PMMA/$TiO_2$ ratio of 1:5. For the LSV testing, similar trend were observed, as shown in Fig. 7b. The photoanode with the PMMA/$TiO_2$ ratio of 1:1 yielded the highest performance in the entire scan range, subsequently followed by the photoanodes with the PMMA/$TiO_2$ ratio of 1:2, 1:5 and 2:1. It is clear that the macropores in the photoanode formed by the PMMA templates functioned as open channels for enhancing the light penetration and mass transfer. Moreover, the enriched macropores, acting as light scattering center, could efficiently increase the light utilization. Therefore, the more macropores were formed, the higher photocurrent density was achieved. However, when the PMMA/$TiO_2$ ratio was too high, because of the film cracking and the deterioration of the solid framework, the electron transfer resistance was increased. In the meantime, the significant amount of macropores led to rather poor contact between the macroporous layer and microporous layer, which also increased the electron transfer resistance. In this case, the possibility of the recombination of photo-generated electron-hole pairs may be also increased. To

further elaborate the underlying mechanism, the EIS measurement of these photoanodes were also performed. Fig. 7c compares the EIS results on the cascading gradient pore microstructured photoanodes with different PMMA/$TiO_2$ ratios. The photoanode with the PMMA/$TiO_2$ ratio of 1:1 was found to show the lowest impedance at low frequency region, while the photoanode with the PMMA/$TiO_2$ ratio of 2:1 exhibited the largest impedance. This result was consistent with the photocurrent and LSV results. It is further confirmed that although high PMMA/$TiO_2$ ratio could enhance mass transport, the resulting electron transfer resistance was also greatly increased, which lowered the photoelectrochemical activity. On the other hand, decreasing the PMMA/$TiO_2$ ratio could facilitate the electron transfer. However, too small PMMA content resulted in less macropores to be formed in the photoanode. In this case, the transport of the photon and ion was resisted, which brought negative effect to the photoelectrochmical reactions. As a result, too high or too low PMMA/$TiO_2$ ratio was not beneficial for the photoanode performance. In our study, an optimal PMMA/$TiO_2$ ratio of 1:1 could yield the best performance because of the minimized charge transfer resistance.

In this work, the effect of the PMMA/$TiO_2$ ratio on the photocatalytic performance of the cascading gradient pore microstructured photoanode was also studied by the MB degradation testing. Fig. 8 shows that the degradation efficiencies with various PMMA/$TiO_2$ ratios after 40 min illumination. As seen, the degradation efficiency was increased from 66.7% to 76.7% when the PMMA/$TiO_2$ ratio increased from 1:5 to 1:1 but became worse when the PMMA/$TiO_2$ ratio was further raised to 2:1. All of them

showed better performance than did the conventional photoanode. The increase of the MB degradation efficiency with increasing the PMMA/$TiO_2$ ratio was attributed to the presence of more macropores, which provided more paths for MB molecules and photons. . However, once the PMMA/$TiO_2$ ratio was too high, as mentioned above, there existed many cracks or defects that decreased mechanical strength. More importantly, the light utilization efficiency was also lowered. Therefore, the degradation efficiency became lower in the case of rather high PMMA/$TiO_2$ ratio. This result indicates that an excessive quantity of the PMMA template is disadvantageous to the photo-degradation of MB. Careful selection of the PMMA/$TiO_2$ ratio is critically important to optimize the performance of the cascading gradient pore microstructured photoanode.

## 4. Conclusions

In this study, a novel photoanode with a cascading gradient pore microstructure has been developed, which consisted of three layers of the nanocrystalline $TiO_2$ layer, the microporous layer and the macroporous layer. The micropores and macropores were fabricated by adding the PEG template and PMMA template into the $TiO_2$ colloid, respectively, while the bottom nanocrystalline $TiO_2$ layer was directly synthesized on FTO conductive glass by the titanium tetraisopropoxide precursor. The SEM images demonstrated that the proposed cascading gradient pore microstructured photoanode was successfully prepared. Enhanced photoelectrochemical activity of the gradient pore microstructured photoanode was verified by the light response, LSV and EIS results in terms of higher photocurrent and low charge transfer resistance compared

with conventional $TiO_2$ photoanode. The developed novel photoanode was also applied to the MB degradation and the testing results demonstrated the enhanced photocatalytic activity of this novel structure. The superiority of the proposed photoanode is mainly attributed to its cascading gradient pore microstructure, which can greatly improve the photon and mass transfer, reduce the electron transfer resistance and prevent the recombination of the photo-generated electron-hole pairs. The study on the effect of the PMMA/$TiO_2$ ratio on the photoanode performance indicated that the photoelectrochemical and photocatalytic activities of the proposed photoanodes were significantly influenced by the PMMA/$TiO_2$ ratio. An increase in the PMMA/$TiO_2$ ratio from 1:5 to 1:1 led to the improved performance because more macropores generated could enhance the mass transport and light harvesting, while too high PMMA/$TiO_2$ ratio worsened the performance because an excessive quantity of the PMMA template resulted in the lowered light utilization efficiency. In short, the cascading gradient pore microstructured photoanode proposed in this work shows a promising prospect for the applications not only in PFCs but also in solar cell, photocatalytic water treatment and other photoelectrochemical systems.

**Acknowledgments**

The authors gratefully acknowledge the financial supports of the National Natural Science Foundation of China (No. 51222603, No. 51276208, No. 51325602 and No. 51576021), the National High Technology Research and Development Program of China (863 Program) (No. 2015AA043503), the Program for New Century Excellent

Talents in University (NCET-12-0591) and the Chongqing Graduate Student Research Innovation Project (No. CYB14012)

**Reference:**

[1] P. Lianos, Production of electricity and hydrogen by photocatalytic degradation of organic wastes in a photoelectrochemical cell, J. Hazard. Mater. 185 (2011) 575–590.

[2] D. Shu, J. Wu, Y. Gong, S. Li, L. Hu, Y. Yang, et al., BiOI-based photoactivated fuel cell using refractory organic compounds as substrates to generate electricity, Cataly. Today. 224 (2014) 13–20.

[3] K. Li, Y. Xu, Y. He, C. Yang, Y. Wang, J. Jia, Photocatalytic fuel cell (PFC) and dye self-photosensitization photocatalytic fuel cell (DSPFC) with BiOCl/Ti photoanode under UV and visible light irradiation, Environ. Sci. Technol. 47 (2013) 3490-3497.

[4] K. Drew, G. Girishkumar, K. Vinodgopal, P.V. Kamat, Boosting fuel cell performance with a semiconductor photocatalyst: $TiO_2$/Pt−Ru hybrid catalyst for methanol oxidation, J. Phys. Chem. B. 109 (2005) 11851–11857.

[5] J. Li, J. Li, Q. Chen, J. Bai, B. Zhou, Converting hazardous organics into clean energy using a solar responsive dual photoelectrode photocatalytic fuel cell, J. Hazard. Mater. 262 (2013) 304–310.

[6] B. Seger, G.Q. Max Lu, L. Wang, Electrical power and hydrogen production from a photo-fuel cell using formic acid and other single-carbon organics, J. Mater. Chem. 22 (2012) 10709–10715.

[7] M. Antoniadou, S. Sfaelou, P. Lianos, Quantum dot sensitized titania for photo-fuel-cell and for water splitting operation in the presence of sacrificial agents, Chem. Eng. J. 254 (2014) 245–251.

[8] Q. Chen, J. Li, X. Li, K. Huang, B. Zhou, W. Cai, et al., Visible-light responsive photocatalytic fuel cell based on $WO_3$/W photoanode and $Cu_2O$/Cu photocathode for simultaneous wastewater treatment and electricity generation, Environ. Sci. Technol. 46 (2012) 11451–11458.

[9] Understanding the performance of optofluidic fuel cells: Experimental and theoretical analyses, Chem. Eng. J. 283 (2016) 1455–1464.

[10] M. Antoniadou, P. Lianos, Production of electricity by photoelectrochemical oxidation of ethanol in a PhotoFuelCell, Appl. Catal. B-Environ. 99 (2010) 307–313.

[11] M. Kaneko, N. Gokan, N. Katakura, Y. Takei, M. Hoshino, Artificial photochemical nitrogen cycle to produce nitrogen and hydrogen from ammonia by platinized $TiO_2$ and its application to a photofuel cell, Chem. Commun. 12 (2005) 1625–1627.

[12] L. Li, G. Wang, R. Chen, X. Zhu, H. Wang, Q. Liao, Y. Yu, Optofluidics based micro-photocatalytic fuel cell for efficient wastewater treatment and electricity generation, Lab Chip. 14 (2014) 3368–3375.

[13] M. Antoniadou, D. Ⅰ. Kondarides, D. Labou, S. Neophytides, P. Lianos, An efficient photoelectrochemical cell functioning in the presence of organic wastes, Sol. Energ. Mat. Sol. C. 94 (2010) 592–597.

[14] B. Liu, E.S. Aydil, Growth of oriented single-crystalline rutile $TiO_2$ nanorods on transparent conducting substrates for dye-sensitized solar cells, J. Am. Chem. Soc. 131 (2009) 3985–3990.

[15] E. Carbonell, F. Ramiro-Manzano, I. Rodríguez, A. Corma, F. Meseguer, H. García, Enhancement of $TiO_2$ photocatalytic activity by structuring the photocatalyst film as photonic sponge, Photochem. Photobiol. Sci. 7 (2008) 931–935.

[16] Y. Liu, J. Li, B. Zhou, S. Lv, X. Li, H. Chen, et al., Photoelectrocatalytic degradation of refractory organic compounds enhanced by a photocatalytic fuel cell, Appl. Catal. B-Environ. 111-112 (2012) 485–491.

[17] B. Wang, H. Zhang, X.-Y. Lu, J. Xuan, M.K.H. Leung, Solar photocatalytic fuel cell using CdS–$TiO_2$ photoanode and air-breathing cathode for wastewater treatment and simultaneous electricity production, Chem. Eng. J. 253 (2014) 174–182.

[18] G. Ai, W. Sun, X. Gao, Y. Zhang, L.-M. Peng, Hybrid CdSe/$TiO_2$ nanowire photoelectrodes: Fabrication and photoelectric performance, J. Mater. Chem. 21 (2011) 8749–8755.

[19] Y. Liu, J. Li, B. Zhou, H. Chen, Z. Wang, W. Cai, A $TiO_2$-nanotube-array-based photocatalytic fuel cell using refractory organic compounds as substrates for electricity generation, Chem. Commun. 47 (2011) 10314–10316.

[20] G. Guan, K. Kusakabe, M. Taneda, M. Uehara, H. Maeda, Catalytic combustion of methane over Pd-based catalyst supported on a macroporous alumina layer in a microchannel reactor, Chem. Eng. J. 144 (2008) 270-276.

[21] T. Kamegawa, N. Suzuki, H. Yamashita, Design of macroporous $TiO_2$ thin film photocatalysts with enhanced photofunctional properties, Energy Environ. Sci. 4 (2011) 1411–1416.

[22] W.J. Zhang, J.W. Bai, PEG and ODA as composite templates to prepare porous TiO2 films by sol-gel method, Appl. Mech. Mater. 63-64 (2011) 698–701.

[23] K.-M. Lee, C.-Y. Hsu, W.-H. Chiu, M.-C. Tsui, Y.-L. Tung, S.-Y. Tsai, et al., Dye-sensitized solar cells with a micro-porous $TiO_2$ electrode and gel polymer electrolytes prepared by in situ cross-link reaction, Sol. Energ. Mater. Sol. C. 93 (2009) 2003–2007.

[24] M. Antoniadou, D.I. Kondarides, D.D. Dionysiou, P. Lianos, Quantum dot sensitized titania applicable as photoanode in photoactivated fuel cells, J. Phys. Chem. C. 116 (2012) 16901–16909.

[25] L. Li, R. Chen, X. Zhu, H. Wang, Y. Wang, Q. Liao, D. Wang. Optofluidic microreactors with $TiO_2$-coated fiberglass, ACS Appl. Mater. Inter. 5 (2013) 12548–12553.

[26] M.I. Mishchenko, Multiple scattering, radiative transfer, and weak localization in discrete random media: unified microphysical approach. Rev. Geophys. 46 (2008) 366-389.

[27] G. Xu, S. Ji, C. Miao, G. Liu, C. Ye, Effect of ZnS and CdS coating on the photovoltaic properties of $CuInS_2$-sensitized photoelectrodes, J. Mater. Chem. 22 (2012) 4890–4896.

[28] Y. Liu, D.-P. Wang, Y.-X. Yu, W.-D. Zhang, Preparation and photoelectrochemical properties of functional carbon nanotubes and Ti co-doped $Fe_2O_3$ thin films, Int. J. Hydrogen Energy. 37 (2012) 9566–9575.

[29] D. Chen, Y. Du, H. Zhu, Y. Deng, Synthesis and characterization of a microfibrous $TiO_2$–CdS/palygorskite nanostructured material with enhanced visible-light photocatalytic activity, Appl. Clay Sci. 87 (2014) 285–291.

## Figure captions

**Figure 1** Schematic of the gradient pore microstructured $TiO_2$ photoanode.

**Figure 2** Cross-sectional SEM images of (a) the prepared NC/$TiO_2$/PMMA photoanode with the PMMA/$TiO_2$ ratio of 1:1; and (b) the nanocrystalline $TiO_2$ layer deposited on the FTO layer.

**Figure 3** Top-view SEM images of (a) the nanocrystalline $TiO_2$ layer; (b) the microporous $TiO_2$ layer; and (c) the macroporous $TiO_2$ layer with the PMMA/$TiO_2$ ratio of 1:1.

**Figure 4** Photoelectrochemical performances of the $TiO_2$, NC/$TiO_2$, NC/PMMA and NC/$TiO_2$/PMMA photoanodes: (a) Light responses; (b) Linear sweep voltammetry; (c) Electrochemical impedance spectra. 10% ethanol and 0.2 M KOH.

**Figure 5** (a) Photocatalytic performances of the $TiO_2$, NC/$TiO_2$, NC/PMMA and NC/$TiO_2$/PMMA photoanodes on the MB degradation; (b) Plot of $-\ln (C_t/C_0)$ versus the irradiation time.

**Figure 6** Top-view and cross-sectional SEM images of the gradient pore microstructured photoanodes with the PMMA/$TiO_2$ ratios of (a) 1:5; (b) 1:2; and (c) 2:1.

**Figure 7** Effect of the PMMA/$TiO_2$ ratio on the photoelectrochemical performance of the gradient pore microstructured photoanode: (a) Light responses; (b) Linear sweep voltammetry; (c) Electrochemical impedance spectra. 10% ethanol and 0.2 M KOH.

**Figure 8** Effect of the PMMA/$TiO_2$ ratio on the photocatalytic performance of the gradient pore microstructured photoanode.

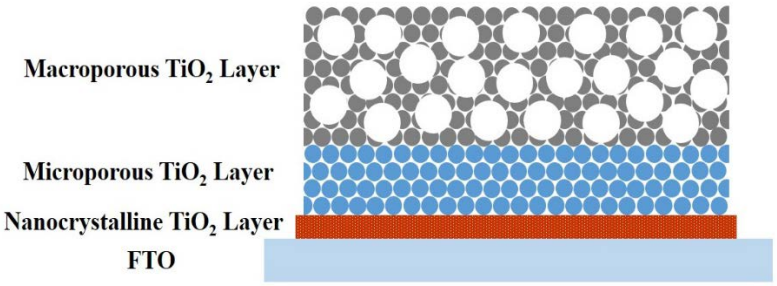


**Fig. 1** Schematic of the cascading gradient pore microstructured $TiO_2$ photoanode.

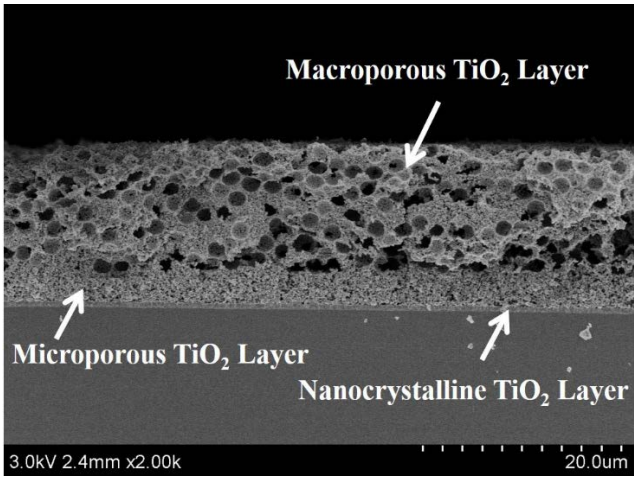


(a)

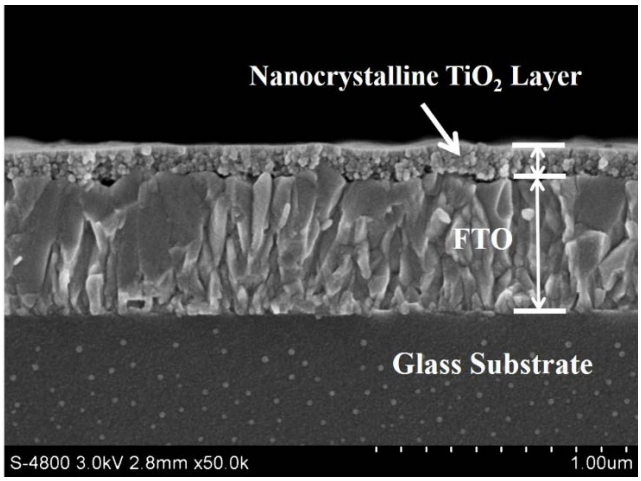


(b)

**Fig. 2** Cross-sectional SEM images of (a) the prepared NC/$TiO_2$/PMMA photoanode with the PMMA/$TiO_2$ ratio of 1:1; and (b) the nanocrystalline $TiO_2$ layer deposited on the FTO layer.

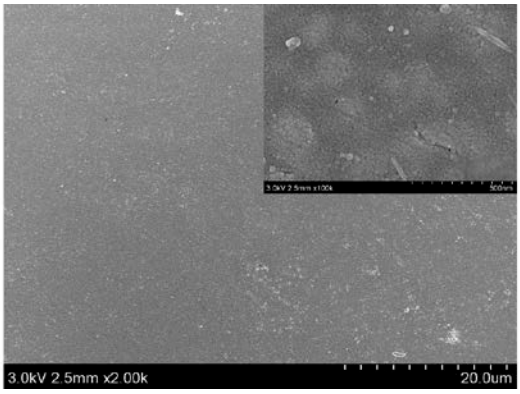


(a)

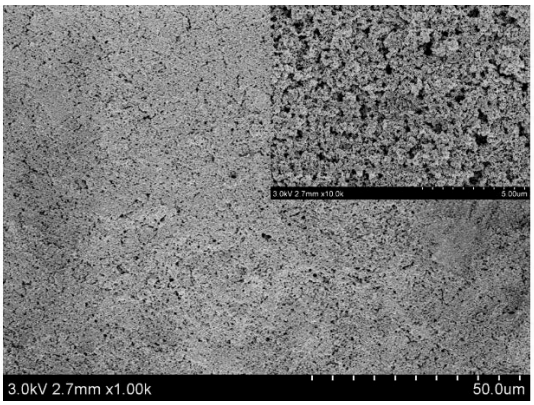


(b)

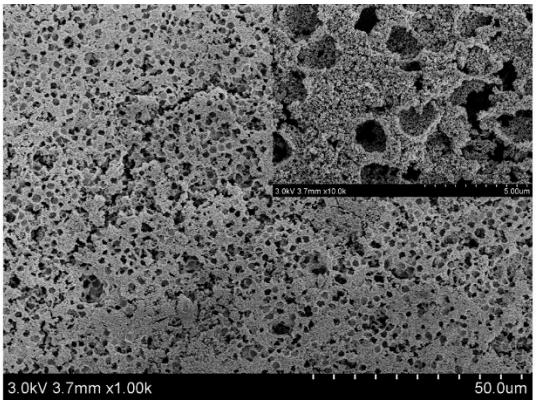


(c)

**Fig. 3** Top-view SEM images of (a) the nanocrystalline $TiO_2$ layer; (b) the microporous $TiO_2$ layer; and (c) the macroporous $TiO_2$ layer with the PMMA/$TiO_2$ ratio of 1:1.

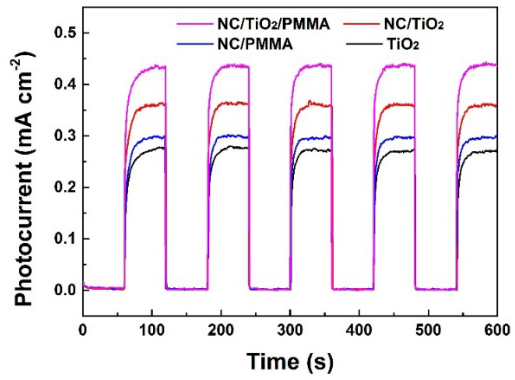


(a)

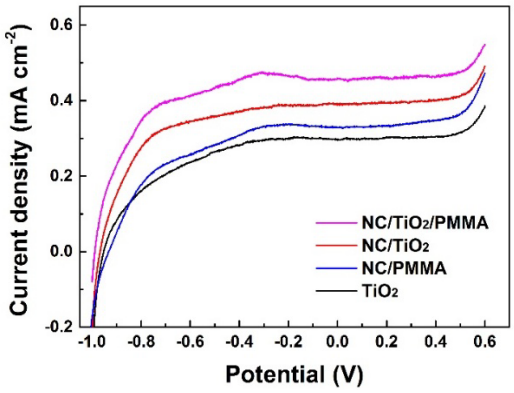


(b)

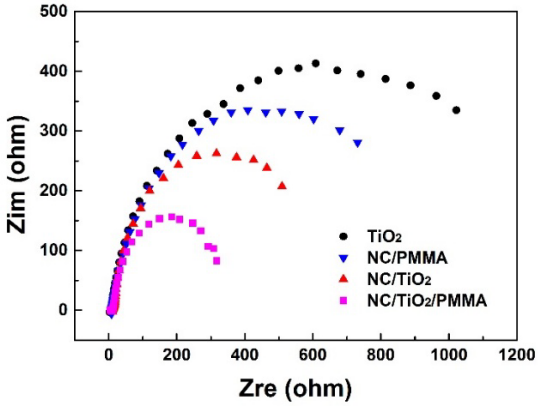


(c)

**Fig. 4** Photoelectrochemical performances of the $TiO_2$, NC/$TiO_2$, NC/PMMA and NC/$TiO_2$/PMMA photoanodes: (a) Light responses; (b) Linear sweep voltammetry; (c) Electrochemical impedance spectra. 10% ethanol and 0.2 M KOH.

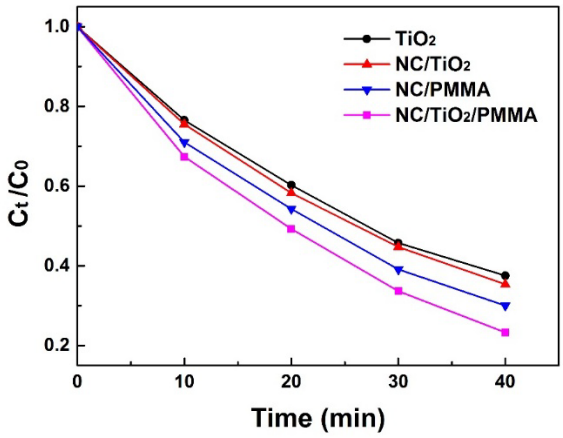


(a)

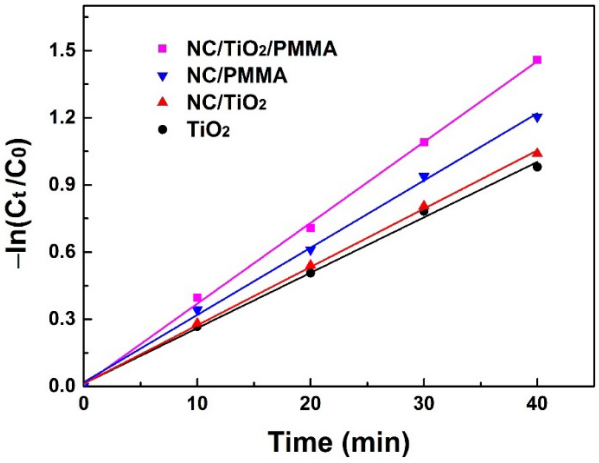


(b)

**Fig. 5** (a) Photocatalytic performances of the $TiO_2$, NC/$TiO_2$, NC/PMMA and NC/$TiO_2$/PMMA photoanodes on the MB degradation; (b) Plot of –ln ($C_t/C_0$) versus the irradiation time.

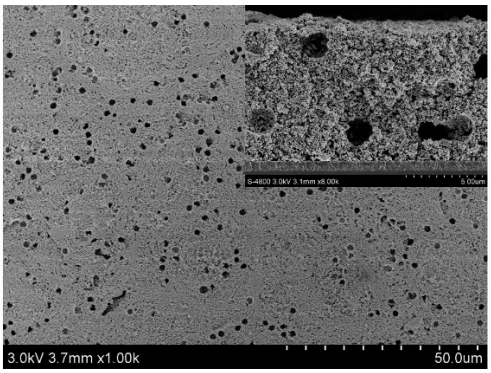


(a)

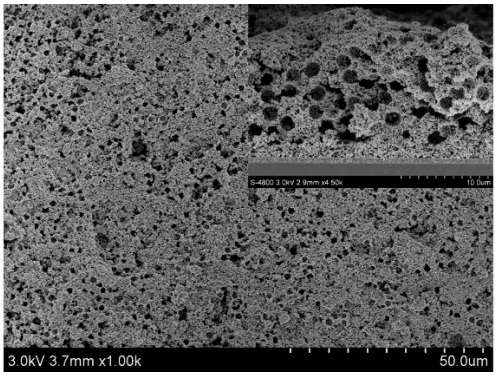


(b)

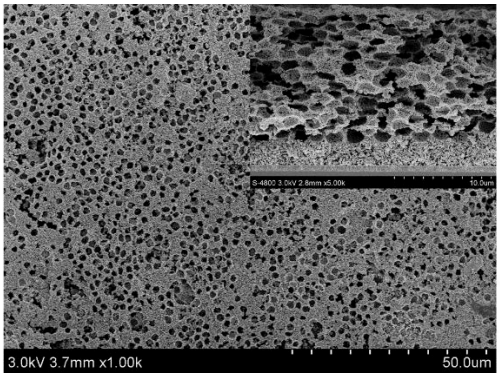


(c)

**Fig. 6** Top-view and cross-sectional SEM images of the cascading gradient pore microstructured photoanodes with the PMMA/$TiO_2$ ratios of (a) 1:5; (b) 1:2; and (c) 2:1.

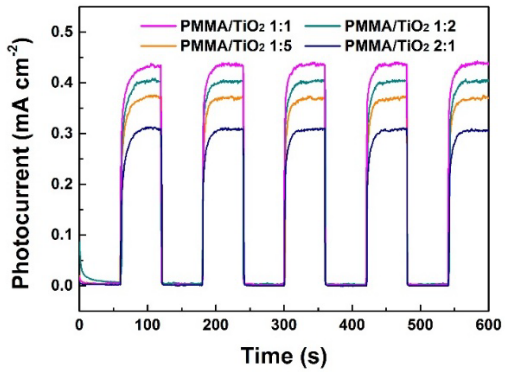


(a)

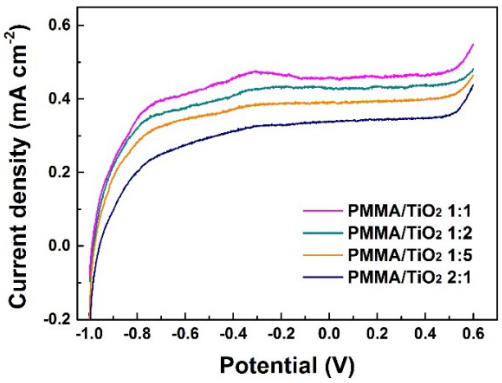


(b)

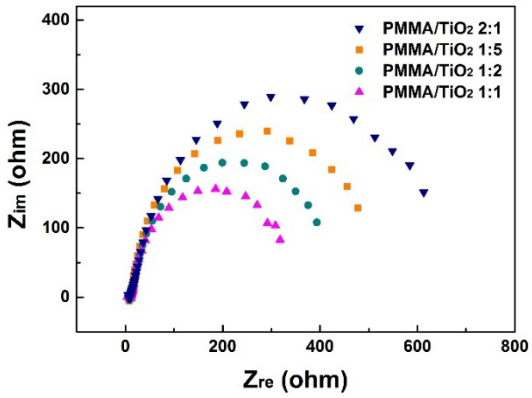


(c)

**Fig. 7** Effect of the PMMA/$TiO_2$ ratio on the photoelectrochemical performance of the cascading gradient pore microstructured photoanode: (a) Light responses; (b) Linear sweep voltammetry; (c) Electrochemical impedance spectra. 10% ethanol and 0.2 M KOH.

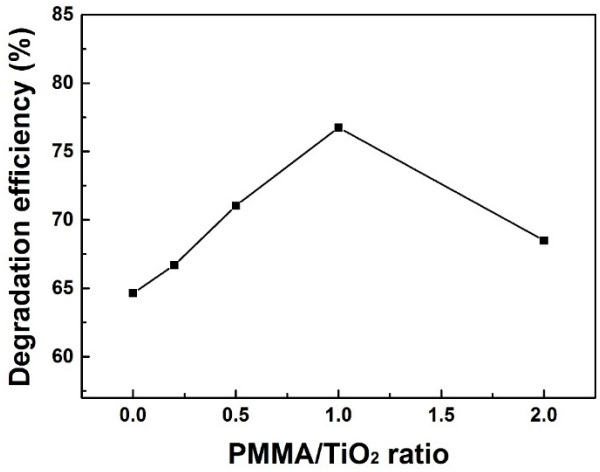


**Fig. 8** Effect of the PMMA/$TiO_2$ ratio on the photocatalytic performance of the cascading gradient pore microstructured photoanode.